

Adaptive Principal Components Allocation with the $\ell_{2,g}$ -regularized Gaussian Graphical Model for Efficient Fine-Tuning Large Models

Jingjing Zheng¹, Yankai Cao^{2,*}

¹Department of Mathematics, The University of British Columbia, BC, Canada

²Chemical and Biological Engineering, The University of British Columbia, BC, Canada

¹jjzheng@math.ubc.ca, ²yankai.cao@ubc.ca

Abstract

In this work, we propose a novel Parameter-Efficient Fine-Tuning (PEFT) approach based on Gaussian Graphical Models (GGMs), marking the first application of GGMs to PEFT tasks, to the best of our knowledge. The proposed method utilizes the $\ell_{2,g}$ -norm to effectively select critical parameters and capture global dependencies. The resulting non-convex optimization problem is efficiently solved using a Block Coordinate Descent (BCD) algorithm. Experimental results on the GLUE benchmark [24] for fine-tuning RoBERTa-Base [18] demonstrate the effectiveness of the proposed approach, achieving competitive performance with significantly fewer trainable parameters. The code for this work is available at: https://github.com/jzheng20/Course_projects.git.

1 Introduction

Recently, various large models, such as BERT [6], Roberta [18], GPT-3 [2], ViT [7], and PaLM [3], have achieved significant success across diverse tasks. Adapting these models for downstream tasks often requires memory-intensive full fine-tuning. To address this, parameter-efficient fine-tuning methods have been developed, such as Prefix-Tuning [17, 19], Adapters [15], Sparse Methods [25, 12], and Low-rank Adaptation (LoRA) [16, 21, 27, 5].

Among them, LoRA [16] has been particularly popular due to its effective reduction of trainable parameters by decomposing the weight increment matrix into two smaller matrices, assuming a low-rank structure. However, it uses a fixed rank r across all layers and modules, which limits flexibility. Some modules might require higher ranks to capture detailed information, while others could use lower ranks to save resources. To address this, AdaLoRA [27] is introduced, in which an importance scoring mechanism is used to adjust the rank based on the contribution of singular values to the training, retaining only the most crucial weights trainable during fine-tuning.

While low-rank methods generally achieve higher parameter efficiency compared to other approaches, they have limitations in capturing global dependencies among param-

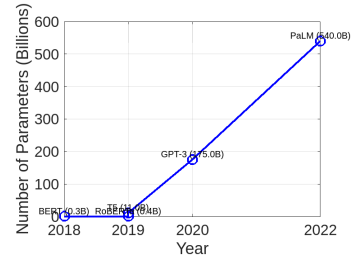


Figure 1: Growth of Large Model Parameters (2018–2022).

eters. For example, AdaLoRA achieves low-rank adaptation through local adjustments of the increment matrices, without capturing the global dependencies among different parameters. In complex downstream tasks, there may be strong interactions among certain parameters that AdaLoRA fails to effectively model. As a result, some critical interactions might be overlooked, potentially compromising the overall effectiveness of fine-tuning in practical applications. Graphical models, such as Gaussian Graphical Models [9, 4, 1], are widely used to explore the dependencies and interactions among variables, making them a natural choice for studying parameter relationships in neural networks.

In this paper, we aim to introduce a novel Parameter-Efficient Fine-Tuning approach based on Gaussian Graphical Model. We answer the following three questions to achieve the goal:

- **Question 1:** How to define the nodes of the graph for the PEFT task?
- **Question 2:** How to define the values of the nodes?
- **Question 3:** How to construct a Gaussian Graphical Model to capture parameter interactions effectively?

Our work has the following two key features:

- (1) Our method utilizes Gaussian Graphical Model to capture the interactions among different trainable parameters for specific downstream tasks. By preserving less critical parameters through freezing and selectively training the more relevant ones, our approach seeks to enhance task-specific adaptation.
- (2) A non-convex surrogate of $\ell_{2,1}$ norm, $\ell_{2,g}$ norm, is used for the structural sparsity regularization and to enforce

*Corresponding author

Symbol	Description
A, B, \dots	Matrices
A_j	The j -th column vector of matrix A
$[A_j]_i$	The i -th element of vector A_j , respectively
$A_{i,j}$	The (i, j) -th element of matrix A
a, b, \dots	Vectors
a_i	The i -th element of vector a , respectively
$\ a\ _2$	The ℓ_2 norm of a , <i>i.e.</i> , $\ a\ _2 = \sqrt{\sum_i a_i^2}$
$\ a\ _1$	The ℓ_1 norm of a , <i>i.e.</i> , $\ a\ _1 = \sum_i a_i $

Table 1: List of symbols.

sparsity at the node level, helping to select the crucial nodes for fine-tuning. To solve the $\ell_{2,g}$ -regularized Gaussian Graphical Model, we propose an optimization algorithm based on the Block Coordinate Descent (BCD) method.

1.1 Conventions

In this paper, we use W_0 to represent a certain weights matrix of a pre-trained large model and ΔW to denote the increment matrix. The symbols and definitions that will be used later in the paper are summarized in the Table 1.

2 The Proposed Methodology

2.1 How to define the nodes and their values?

In this section, we address the first two questions raised in the Introduction.

For large models, which often consist of billions of parameters, defining nodes on an element-wise basis is impractical. Fortunately, over-parameterized models tend to exhibit low-rank properties in their weight matrices. Figure 2.1 illustrates the frequency distribution of singular values for the 5-th projection weight matrix of the query in RoBERTa-base and RoBERTa-large. As shown in the figure, most singular values are small and close to zero. Inspired by this observation, we propose selecting the most significant r principal components and the bias for each layer as the nodes.

Node Definition

Let $W_0 = USV^\top$ represent the weight matrix of a specific layer, where U , S , and V are obtained by the Singular Value Decomposition (SVD) of W_0 . Define $A_i = S_{i,i}U_i$ and $B_i = V_i^\top$, where $S_{i,i}$, U_i , and V_i correspond to the i -th singular value, and its associated left and right singular vectors, respectively. We define $r + 1$ nodes of that layer as $(A_1, B_1), (A_2, B_2), \dots, (A_r, B_r), b$, where b is the bias of the layer. Assuming the model has h layers, we select r principal components per layer results in a total of $h(r + 1)$ nodes.

Node Value Calculation

We use the importance score $s^{(k)}(\cdot)$ [26] to calculate the values of the nodes and defined as

$$s^{(k)}(W_{i,j}) = \bar{I}^{(k)}(W_{i,j}) \cdot \bar{U}^{(k)}(W_{i,j}), \quad (1)$$

where

$$\bar{I}^{(k)}(W_{i,j}) = \beta_1 \bar{I}^{(k-1)}(W_{i,j}) + (1 - \beta_1) I^{(k)}(W_{i,j}),$$

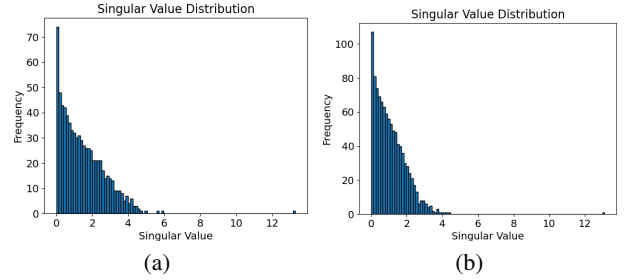


Figure 2: Illustration of the low-rank property in the learned over-parametrized models for (a) Roberta-base (Query) and (b) Roberta-large (Query).

$$\begin{aligned} \bar{U}^{(k)}(W_{i,j}) &= \beta_2 \bar{U}^{(k-1)}(W_{i,j}) \\ &\quad + (1 - \beta_2) |I^{(k)}(W_{i,j}) - \bar{I}^{(k)}(W_{i,j})|, \end{aligned}$$

and

$$I(W_{i,j}) = |W_{i,j} \nabla_{W_{i,j}} \mathcal{L}|.$$

A high $I(W_{i,j})$ indicates that $W_{i,j}$ has a greater impact on the loss function.

Using the importance score $s^{(k)}(\cdot)$, we calculate the node values as follows:

- For (A_i, B_i) :

$$\begin{aligned} v^{(k)}((A_i, B_i)) &= \frac{1}{2d_1} \sum_{j=1}^{d_1} s^{(k)}([A_i]_j) \\ &\quad + \frac{1}{2d_2} \sum_{j=1}^{d_2} s^{(k)}([B_i]_j) \quad (2) \end{aligned}$$

where d_1 and d_2 represent the dimensions of A_i and B_i , respectively.

- For b :

$$v^{(k)}(b) = \frac{1}{2d_2} \sum_{j=1}^{d_2} s^{(k)}(b_j). \quad (3)$$

Here, k refers to the training step, and different samples are obtained for different k .

2.2 The Proposed Gaussian Graphical Model

The $\ell_{2,1}$ -regularized Gaussian Graphical Model

Unlike graphical lasso, which focuses on edge sparsity (*i.e.*, the relationships between individual nodes), the goal of this-work is to select nodes by learning a structure where a small subset of nodes exhibits stronger interactions with all other nodes. Instead of emphasizing edge connections, we focus on the interaction strength of each node with the remaining nodes. To achieve this, we introduce structural sparsity regularization for the precision matrix $\Omega \in \mathbb{R}^{n \times n}$. Specifically, we measure the interaction strength between node i and all other nodes using $\|\hat{\Omega}_i\|_2$, where

$$\hat{\Omega}_i = [\Omega_{1,i}, \Omega_{2,i}, \dots, \Omega_{i-1,i}, \Omega_{i+1,i}, \dots, \Omega_{n,i}]^\top \in \mathbb{R}^{n-1}.$$

Name	$g(x)$
ℓ_p	$x^p, 0 < p < 1$
Geman	$\frac{x}{x+\epsilon}$
Laplace	$(1 - \exp(-\frac{x}{\gamma}))$
LOG	$\log(\gamma + x)$
Logarithm	$\frac{1}{\log(\gamma+1)} \log(\gamma x + 1)$
ETP	$\frac{1 - \exp(-\gamma x)}{1 - \exp(-\gamma)}$

Table 1: Examples of surrogate functions of ℓ_0 norm.

Consequently, we adopt the $\ell_{2,1}$ -norm of $\hat{\Omega}$:

$$\|\hat{\Omega}\|_{2,1} = \sum_{i=1}^n \|\hat{\Omega}_i\|_2,$$

instead of the traditional ℓ_1 -norm, to better capture these structural interactions. Based on this formulation, we propose the following Gaussian Graphical Model:

$$\max_{\Omega \succeq 0} \left(\log \det \Omega - \langle \hat{\Sigma}, \Omega \rangle - \tau \|\hat{\Omega}\|_{2,1} \right), \quad (4)$$

where $\hat{\Sigma}$ is the sample covariance matrix, $\Omega \in \mathbb{R}^{n \times n}$, and $\|\hat{\Omega}\|_{2,1} = \sum_j \|\hat{\Omega}_j\|_2$.

The $\ell_{2,1}$ -regularized Gaussian Graphical Model with “Important Nodes”

Although the regularization in (4) effectively promotes structural sparsity, it loses information about the magnitude of the importance scores. This limitation arises because the sample mean is subtracted during the computation of the sample covariance matrix. The sample mean, however, contains crucial information for the Parameter-Efficient Fine-Tuning (PEFT) task. Beyond selecting nodes with strong interactions, it is also essential to prioritize nodes with relatively large values.

Therefore, we introduce the concept of “important nodes”, which are nodes with a significant impact on the loss function. Let $\mathbb{I} = \{i_1, i_2, \dots, i_h\}$ represent the set of “important nodes.” We measure the interaction strength between node i ($i \notin \mathbb{I}$) and the nodes in \mathbb{I} using $\|\bar{\Omega}_i\|_2$, where

$$\bar{\Omega}_i = [\Omega_{i_1, i}, \Omega_{i_2, i}, \dots, \Omega_{i_h, i}]^\top \in \mathbb{R}^h.$$

Based on this concept, we derive a modified $\ell_{2,1}$ -regularization term:

$$\|\bar{\Omega}\|_{2,1} = \sum_{j \notin \mathbb{I}} \|\bar{\Omega}_j\|_2,$$

and proposed the following improved model:

$$\max_{\Omega \succeq 0} \left(\log \det \Omega - \langle \hat{\Sigma}, \Omega \rangle - \tau \|\bar{\Omega}\|_{2,1} \right). \quad (5)$$

In this work, the set \mathbb{I} is determined by selecting the nodes with the highest values in the sample mean.

2.3 The $\ell_{2,g}$ -regularized Gaussian Graphical Model

The ℓ_1 -norm of $v = [\|\bar{\Omega}_{i_1}\|_2, \|\bar{\Omega}_{i_2}\|_2, \dots, \|\bar{\Omega}_{i_h}\|_2]$, serves as the convex relaxation of the ℓ_0 norm and is widely used

Algorithm 1: Adaptive Principal Components Allocation with the $\ell_{2,g}$ -regularized Gaussian Graphical Model

Input: Pre-trained weight matrices, r

1. Reparameterize the pre-trained weight matrices using SVD and extract the principal components as nodes.
 2. Set the extracted nodes as trainable and freeze the residual components.
 3. Collect samples during the initial stages of the training process for the large model.
 4. Compute the sample mean and identify \mathbb{I} , the set of nodes corresponding to the highest values in the sample mean.
 5. Solve the proposed $\ell_{2,g}$ -regularized Gaussian Graphical Model to obtain Ω^* .
 6. Continue training the nodes in \mathbb{I} and those with large $\|\Omega_i^*\|_2$, while freezing the remaining nodes.
-

to induce sparsity in v for optimization problems like (5). However, the ℓ_1 -norm often fails to produce truly sparse solutions. Achieving effective sparsity generally requires increasing the regularization parameter, which may lead to over-penalization for the solution.

A common solution in low-rank and sparse learning is to adopt a non-convex strategy, replacing $|\cdot|$ with surrogate functions $g(\cdot)$. This approach balances solvability and effectiveness, enabling genuinely sparse solutions. Incorporating this modification transforms the optimization problem into a non-convex formulation, expressed as follows:

$$\max_{\Omega \succeq 0} \left(\log \det \Omega - \langle \hat{\Sigma}, \Omega \rangle - \tau \|\bar{\Omega}\|_{2,g} \right), \quad (6)$$

where $\|\bar{\Omega}\|_{2,g} = \sum_{j \notin \mathbb{I}} g(\|\bar{\Omega}_j\|_2)$, and $g(x)$ is non-negative, increasing, and concave for $x \geq 0$.

Therefore, we developed a PEFT method utilizing the $\ell_{2,g}$ -regularized Gaussian Graphical Model, as outlined in the Algorithm 1.

3 Optimization by Block Coordinate Descent (BCD) for the Proposed $\ell_{2,g}$ -regularized Model

Since the optimization problem in (6) is non-convex and challenging to solve directly, we propose an optimization algorithm based on the Block Coordinate Descent (BCD) method [28, 14]. To simplify (6) for BCD, we reformulate it as follows.

We first introduce an auxiliary variable Δ such that $\Delta = \Omega$, leading to the equivalent problem:

$$\max_{\Omega > 0, \Delta = \Omega} \left(\log \det \Omega - \langle \hat{\Sigma}, \Omega \rangle - \tau \|\bar{\Delta}\|_{2,g} \right).$$

To remove the equality constraint $\Delta = \Omega$, we add a penalty term $-\lambda \|\Omega - \Delta\|_F^2$, encouraging Δ to stay close to Ω . This leads to the following reformulated problem:

$$\max_{\Omega > 0} \left(\log \det \Omega - \langle \hat{\Sigma}, \Omega \rangle - \lambda \|\Omega - \Delta\|_F^2 - \tau \|\bar{\Delta}\|_{2,g} \right), \quad (7)$$

Algorithm 2: Block Coordinate Descent

Input: $\hat{\Sigma} \succeq 0, \mathbb{I}, \lambda > 0, \tau > 0, g(\cdot)$
Output: $\Omega^T \succeq 0$
Initialize $\Omega^{(0)} = \text{diag}(\hat{\Sigma})^{-1}$;
for each iteration $t = 1, \dots, T$ **do**
 1. Update $\Omega^{(t+1)}$ **for given** $\Delta^{(t)}$:
 $\Omega^{(t+1)} = \arg \max_{\Omega \succeq 0} \left(\frac{1}{2\lambda} \log \det \Omega - \langle \frac{A+A^\top}{2}, \Omega \rangle - \frac{1}{2} \|\Omega\|_F^2 \right), A = \frac{\hat{\Sigma} - 2\lambda \Delta^{(t)}}{2\lambda}$;
 2. Update $\Delta^{(t+1)}$ **for given** $\Omega^{(t+1)}$:
 for $i = 1, \dots, n$ **do**
 if $i \in \mathbb{I}$ **then**
 $\Delta_i = \Omega_i^{(t+1)}$;
 else
 $\alpha^* = \arg \min_{\alpha} \left(\frac{1}{2} (\|\bar{\Omega}_i^{(t+1)}\|_2 - \alpha)^2 + \frac{\tau}{2\lambda} g(|\alpha|) \right)$;
 $\Delta_{j,i}^{(t+1)} = \Omega_{j,i}^{(t+1)}$ **for** $j \notin \mathbb{I}$,
 $\bar{\Delta}_i^{(t+1)} = \alpha^* \frac{\bar{\Omega}_i^{(t+1)}}{\|\bar{\Omega}_i^{(t+1)}\|_2}$.
 end
 end
end

where $\lambda > 0$. As $\lambda \rightarrow +\infty$, Δ converges to Ω .

Using the BCD framework, we alternately optimize Ω and Δ as follows:

$$\begin{cases} \Omega^{(t+1)} = \arg \max_{\Omega \succ 0} \left(\log \det \Omega - \langle \hat{\Sigma}, \Omega \rangle - \lambda \|\Omega - \Delta^{(t)}\|_F^2 \right); \\ \Delta^{(t+1)} = \arg \max_{\Delta} \left(-\lambda \|\Omega^{(t+1)} - \Delta\|_F^2 - \tau \|\bar{\Delta}\|_{2,g} \right). \end{cases} \quad (9)$$

It is important to note that, while the second subproblem is non-convex, it has been well-studied in the field of low-rank sparse representation. By leveraging the Block Coordinate Descent (BCD) approach, we can effectively decompose a more complex problem (6) into two simpler subproblems. Below, we detail the solutions to these two subproblems.

3.1 The Updating of the Precision Matrix

For a given $\Delta^{(t)}$, we update $\Omega^{(t+1)}$ by solving

$$\begin{aligned} & \max_{\Omega \succ 0} \left(\frac{1}{2\lambda} \log \det \Omega - \langle \frac{\hat{\Sigma}}{2\lambda}, \Omega \rangle - \frac{1}{2} \|\Omega - \Delta^{(t)}\|_F^2 \right) \\ &= \max_{\Omega \succ 0} \left(\frac{1}{2\lambda} \log \det \Omega - \langle \frac{\hat{\Sigma}}{2\lambda} - \Delta^{(t)}, \Omega \rangle - \frac{1}{2} \|\Omega\|_F^2 \right) \\ &= \max_{\Omega \succ 0} \left(\frac{1}{2\lambda} \log \det \Omega - \langle A_s, \Omega \rangle - \frac{1}{2} \|\Omega\|_F^2 \right), \end{aligned} \quad (8)$$

where $A = \frac{\hat{\Sigma}}{2\lambda} - \Delta^{(t)}$ and $A_s = \frac{1}{2}(A + A^\top)$. Since (8) is concave, it can be solved using gradient descent with the following update rule:

$$\Omega^{(k+1)} = \Omega^{(k)} + \eta \left(\frac{1}{2\lambda} (\Omega^{(k)})^{-1} - A_s - \Omega^{(k)} \right),$$

where $\eta > 0$ is the learning rate.

Algorithm 3: Generalized Accelerating Iterative Algorithm (GAI) [28]

Input: A real number $y > 0$, a threshold $\lambda > 0$, and a tolerance $\tau > 0$.

Output: $T_g(y, \lambda) = x_G^*$.

Let

$$\begin{cases} f_y(x) = \frac{1}{2}(y-x)^2 + \lambda g(x), \\ J_1(x) = y - \lambda g'(x), \\ J_2(x) = J_1(x) - \frac{(J_1(J_1(x)) - J_1(x))(J_1(x) - x)}{J_1(J_1(x)) - 2J_1(x) + x}. \end{cases}$$

$a_0 \leftarrow \max\{x \mid J_1'(x) = 1 \text{ or } x = 0\}$.

if $f_y'(a_0) < 0$ **then**

 // Find \hat{x}_G by fixed point iteration

 Initialize $x_G^{(0)} \leftarrow y, t \leftarrow 0$

while $|J_1(J_1(x_G^{(t)})) - 2J_1(x_G^{(t)}) + x_G^{(t)}| > \tau$ **do**

$x_G^{(t+1)} = J_2(x_G^{(t)})$

$t \leftarrow t + 1$

$\hat{x}_G = J_1(x_G^{(t)})$

else

return $\hat{x}_G = a_0$

If $f_y(0) > f_y(\hat{x}_G)$, **return** $x_G^* = \hat{x}_G$; **otherwise return** $x_G^* = 0$.

3.2 The Updating of the Auxiliary Variable

For given $\Omega^{(t+1)}$, we update $\Delta^{(t+1)}$ by solving

$$\begin{aligned} & \min_{\Delta} \left(\frac{1}{2} \|\Omega^{(t+1)} - \Delta\|_F^2 + \frac{\tau}{2\lambda} \|\bar{\Delta}\|_{2,g} \right) \\ &= \min_{\Delta} \left(\frac{1}{2} \|\Omega^{(t+1)} - \Delta\|_F^2 + \frac{\tau}{2\lambda} \sum_{j \notin \mathbb{I}} g(\|\bar{\Delta}_j\|_2) \right). \end{aligned} \quad (9)$$

Since the optimization for each column of Δ is independent, we solve Δ_i separately:

- For $i \in \mathbb{I}$,

$$\min_{\Delta_i} \left(\frac{1}{2} \|\Omega_i^{(t+1)} - \Delta_i\|_F^2 \right),$$

which leads to the solution $\Delta_i = \Omega_i^{(t+1)}$.

- For $i \notin \mathbb{I}$, we optimize Δ_i by

$$\begin{aligned} & \min_{\Delta_i} \left(\left(\frac{1}{2} \|\bar{\Omega}_i^{(t+1)} - \bar{\Delta}_i\|_F^2 + \frac{\tau}{2\lambda} g(\|\bar{\Delta}_i\|_2) \right) \right. \\ & \quad \left. + \frac{1}{2} \sum_{j \notin \mathbb{I}} (\Omega_{j,i}^{(t+1)} - \Delta_{j,i})^2 \right) \end{aligned} \quad (10)$$

and it leads to

$$\begin{cases} \Delta_{j,i} = \Omega_{j,i}^{(t+1)} \text{ for } j \notin \mathbb{I}; \\ \bar{\Delta}_i = \alpha^* \frac{\bar{\Omega}_i^{(t+1)}}{\|\bar{\Omega}_i^{(t+1)}\|_2}, \end{cases}$$

where

$$\alpha^* \in T_g(\|\bar{\Omega}_i^{(t+1)}\|_2, \frac{\tau}{2\lambda}) = \arg \min_{\alpha} \left(\frac{1}{2} (\|\bar{\Omega}_i^{(t+1)}\|_2 - \alpha)^2 + \frac{\tau}{2\lambda} g(|\alpha|) \right). \quad (11)$$

Method	# Trainable Parameters	SST-2	MRPC	CoLA	STS-B	Avg.
		Acc.	Acc.	MCC	PCC	
FF	125M	94.8	90.2	<u>63.6</u>	<u>91.2</u>	<u>85.0</u>
LoRA	0.3M	<u>95.1</u>	89.7	63.4	91.5	84.9
AdaLoRA	0.3M	94.5	88.7	62.0	90.5	83.9
DyLoRA	0.3M	94.3	89.5	61.1	91.1	84.0
PiSSA ^F	<u>0.248M</u>	93.6	89.3	62.2	90.0	83.8
Ours-2	0.084M	95.2	90.2	64.4	90.4	85.1

Table 2: The performance comparison of various fine-tuning methods on four datasets (SST-2, MRPC, CoLA, and STS-B) from the GLUE benchmark using the RoBERTa-Base model. Metrics used include accuracy (Acc.) for SST-2 and MRPC, Matthews Correlation Coefficient (MCC) for CoLA, and Pearson Correlation Coefficient (PCC) for STS-B. ‘‘Ours-2’’ represents the proposed method with ‘‘important nodes’’. Results are averaged over five random seeds {0, 11111, 22222, 33333, 44444}.

Method	MRPC	CoLA	STS-B
Ours-1	89.2	64.8	90.2
Ours-2	90.2	65.1	90.4

Table 3: Ablation Study: ‘‘Ours-1’’ stands for the proposed method without ‘‘important nodes’’. All results in this table are based on random seed 0.

A general solver for $T_g(\|\bar{\Omega}_i^{(t+1)}\|_2, \frac{\tau}{2\lambda})$, which converges to the global optimal solution with a superlinear rate, is provided in Algorithm 3.

4 Experiments

In the experiments, we compared the proposed methods (Ours-1 and Ours-2) with following SOTA PEFT methods: **Fully Fine-tuning (FF)**, **LoRA** [16], **AdaLoRA** [27], **DyLoRA** [23], and **PiSSA** [21] on Natural Language Understanding tasks, where **LoRA**, **AdaLoRA**, **DyLoRA**, and **PiSSA** are the matrix-based methods. The GLUE benchmark [24] for the RoBERTa-Base [18] is used for evaluation. Three key metrics including Matthew’s correlation coefficient (MCC), Pearson correlation coefficient (PCC), and accuracy (Acc.) are used to evaluate the performance of different fine-tuned models for CoLA, STS-B, and all other tasks, respectively. Consistent with [12], we limit the training to a maximum of 100 epochs and select the best-performing epoch for each run. All experimental results are summarized in Tables 2-3. The best results for each case are highlighted in bold, while the second-best results are underlined. From the results shown in Table 2, it is evident that the proposed method achieves comparable performance while using significantly fewer trainable parameters, demonstrating the parameter efficiency of the proposed approach. Furthermore, the comparison between Ours-1 and Ours-2 in Table 3 highlights the importance of the introduced concept of ‘‘important nodes.’’

5 Conclusion

In this work, we proposed a novel approach to Parameter-Efficient Fine-Tuning (PEFT) by using Gaussian Graphical Models. To the best of our knowledge, the first attempt to apply this methodology in the context of PEFT tasks. Our method demonstrates significant parameter efficiency, utilizing far fewer trainable parameters than existing methods while maintaining competitive performance. This highlights

the potential of Gaussian Graphical Models in achieving both effectiveness and efficiency in fine-tuning large models.

This work is still ongoing, we plan to conduct further ablation studies and extend our experiments to larger models to strengthen and validate our findings. Additionally, going beyond focus on backpropagation, we aim to explore the contribution of each node during forward propagation to deepen our understanding and enhance the interpretability of large models.

References

- [1] Céline Brouard, Simon de Givry, and Thomas Schiex. Pushing data into cp models using graphical model learning and solving. In Helmut Simonis, editor, *Principles and Practice of Constraint Programming*, pages 811–827. Springer International Publishing, 2020.
- [2] Tom B. Brown, Benjamin Mann, Nick Ryder, Melanie Subbiah, and et al. Language models are few-shot learners. 2020.
- [3] Aakanksha Chowdhery, Sharan Narang, Jacob Devlin, Maarten Bosma, and et al. Palm: scaling language modeling with pathways, 2022.
- [4] Junwei Lu Cong Ma and Han Liu. Inter-subject analysis: A partial gaussian graphical model approach. *Journal of the American Statistical Association*, 116(534):746–755, 2021.
- [5] Tim Dettmers, Artidoro Pagnoni, Ari Holtzman, and Luke Zettlemoyer. Qlora: efficient finetuning of quantized llms. *Advances in Neural Information Processing Systems*, 36, 2024.
- [6] Jacob Devlin, Ming-Wei Chang, Kenton Lee, and Kristina Toutanova. Bert: pre-training of deep bidirectional transformers for language understanding, 2019.
- [7] Alexey Dosovitskiy, Lucas Beyer, Alexander Kolesnikov, Dirk Weissenborn, Xiaohua Zhai, Thomas Unterthiner, Mostafa Dehghani, Matthias Minderer, Georg Heigold, Sylvain Gelly, et al. An image is worth 16x16 words: transformers for image recognition at scale. *arXiv preprint arXiv:2010.11929*, 2020.
- [8] LLdiko E Frank and Jerome H Friedman. A statistical view of some chemometrics regression tools. *Technometrics*, 35(2):109–135, 1993.
- [9] Jerome Friedman, Trevor Hastie, and Robert Tibshirani. Sparse inverse covariance estimation with the graphical lasso. *Biostatistics*, 9(3):432–441, 2007.

- [10] Jerome H Friedman. Fast sparse regression and classification. *International Journal of Forecasting*, 28(3):722–738, 2012.
- [11] Cuixia Gao, Naiyan Wang, Qi Yu, and Zhihua Zhang. A feasible nonconvex relaxation approach to feature selection. In *Proceedings of the AAAI Conference on Artificial Intelligence*, volume 25, pages 356–361, 2011.
- [12] Ziqi Gao, Qichao Wang, Aochuan Chen, Zijing Liu, Bingzhe Wu, Liang Chen, and Jia Li. Parameter-efficient fine-tuning with discrete fourier transform. *arXiv preprint arXiv:2405.03003*, 2024.
- [13] Donald Geman and Chengda Yang. Nonlinear image recovery with half-quadratic regularization. *IEEE transactions on Image Processing*, 4(7):932–946, 1995.
- [14] Jean Honorio, Dimitris Samaras, Irina Rish, and Guillermo Cecchi. Variable selection for gaussian graphical models. In *Artificial Intelligence and Statistics*, pages 538–546. PMLR, 2012.
- [15] Neil Houlsby, Andrei Giurgiu, Stanislaw Jastrzebski, Bruna Morrone, Quentin de Laroussilhe, Andrea Gesmundo, Mona Attariyan, and Sylvain Gelly. Parameter-efficient transfer learning for nlp, 2019.
- [16] Edward J Hu, Yelong Shen, Phillip Wallis, Zeyuan Allen-Zhu, Yuanzhi Li, Shean Wang, Lu Wang, and Weizhu Chen. Lora: low-rank adaptation of large language models. *arXiv preprint arXiv:2106.09685*, 2021.
- [17] Xiang Lisa Li and Percy Liang. Prefix-tuning: optimizing continuous prompts for generation. *arXiv preprint arXiv:2101.00190*, 2021.
- [18] Yinhan Liu, Myle Ott, Naman Goyal, Jingfei Du, Mandar Joshi, Danqi Chen, Omer Levy, Mike Lewis, Luke Zettlemoyer, and Veselin Stoyanov. Roberta: a robustly optimized bert pretraining approach, 2019.
- [19] Xiao Liu, Kaixuan Ji, Yicheng Fu, Weng Lam Tam, Zhengxiao Du, Zhilin Yang, and Jie Tang. P-tuning v2: prompt tuning can be comparable to fine-tuning universally across scales and tasks, 2022.
- [20] Dmitry Malioutov and Aleksandr Aravkin. Iterative log thresholding, 2013.
- [21] Fanxu Meng, Zhaohui Wang, and Muhan Zhang. Pissa: principal singular values and singular vectors adaptation of large language models. *arXiv preprint arXiv:2404.02948*, 2024.
- [22] Joshua Trzasko and Armando Manduca. Highly under-sampled magnetic resonance image reconstruction via homotopic ℓ_0 -minimization. *IEEE Transactions on Medical Imaging*, 28(1):106–121, 2008.
- [23] Mojtaba Valipour, Mehdi Rezagholizadeh, Ivan Kobzyev, and Ali Ghodsi. Dylora: parameter efficient tuning of pre-trained models using dynamic search-free low-rank adaptation. *arXiv preprint arXiv:2210.07558*, 2022.
- [24] Alex Wang, Amanpreet Singh, Julian Michael, Felix Hill, Omer Levy, and Samuel R Bowman. Glue: a multi-task benchmark and analysis platform for natural language understanding. *arXiv preprint arXiv:1804.07461*, 2018.
- [25] Elad Ben Zaken, Shauli Ravfogel, and Yoav Goldberg. Bitfit: simple parameter-efficient fine-tuning for transformer-based masked language-models, 2022.
- [26] Qingru Zhang, Simiao Zuo, Chen Liang, Alexander Bukharin, Pengcheng He, Weizhu Chen, and Tuo Zhao. Platon: Pruning large transformer models with upper confidence bound of weight importance. In *International conference on machine learning*, pages 26809–26823. PMLR, 2022.
- [27] Qingru Zhang, Minshuo Chen, Alexander Bukharin, Nikos Karampatziakis, Pengcheng He, Yu Cheng, Weizhu Chen, and Tuo Zhao. Adalora: adaptive budget allocation for parameter-efficient fine-tuning. *arXiv preprint arXiv:2303.10512*, 2023.
- [28] Xiaoqin Zhang, Jingjing Zheng, Di Wang, Guiying Tang, Zhengyuan Zhou, and Zhouchen Lin. Structured sparsity optimization with non-convex surrogates of $\ell_{2,0}$ -norm: A unified algorithmic framework. *IEEE Transactions on Pattern Analysis and Machine Intelligence*, 45(5):6386–6402, 2023.